



ELSEVIER

Available online at [www.sciencedirect.com](http://www.sciencedirect.com)

SCIENCE @ DIRECT®

Proceedings of the Combustion Institute 30 (2005) 1293–1300

Proceedings  
of the  
Combustion  
Institute

[www.elsevier.com/locate/proci](http://www.elsevier.com/locate/proci)

# Species reconstruction using pre-image curves

Zhuyin Ren\*, Stephen B. Pope

*Sibley School of Mechanical and Aerospace Engineering, Cornell University, Ithaca, NY 14853, USA*

## Abstract

All chemistry dimension-reduction methodologies, such as quasi-steady-state approximation (QSSA), rate-controlled constrained equilibrium (RCCE), and intrinsic low-dimensional manifolds (ILDM), either implicitly or explicitly, provide a means of *species reconstruction*. Given a reduced description of the chemical composition (e.g., in terms of some “major” species), species reconstruction is a procedure to estimate the full composition. In this paper, we develop and demonstrate a new species reconstruction methodology, which is based on a pre-image curve of the reaction mapping. By definition, in the composition space, if a reaction trajectory is followed from any point on the pre-image curve, then at some time the reduced composition on the trajectory intersects the given reduced composition. The reconstructed composition is taken to be the full composition on the reaction trajectory at this intersection. The method is tested for a case of methane autoignition in which the detailed mechanism has 27 degrees of freedom, and two reduced descriptions are considered with 4 and 6 degrees of freedom. It is shown that the normalized reconstruction errors are very small; they are two orders of magnitude smaller than those in RCCE; and with 6 degrees of freedom they are smaller than those in QSSA with 12 degrees of freedom. The reconstructed compositions (for all reduced compositions) form the reconstructed manifold. It is shown that, to an excellent approximation, this manifold is inertial (i.e., it is composed of reaction trajectories). In comparison to other dimension-reduction methodologies, this is the first approach which determines, locally, points on a low-dimensional inertial manifold. The combination of in situ adaptive tabulation and species reconstruction can be used to reduce substantially the computational cost of applying detailed chemistry to turbulent combustion calculations.

© 2004 The Combustion Institute. Published by Elsevier Inc. All rights reserved.

*Keywords:* Dimension reduction; Reduced chemistry

## 1. Introduction

Substantial advances continue to be made in our abilities to simulate turbulent combustion. Yet for hydrocarbon fuels, the computational cost of directly using detailed chemical kinetics is large and usually prohibitive. The computational cost of using the detailed chemical information in turbulent combustion simulations can be dramati-

cally reduced by exploiting, in combination, techniques of dimension reduction and storage retrieval. For example, recent probability density functional (PDF) calculations of turbulent methane flames performed in our group [1] have used a 19-species reduced mechanism [2], implemented using in situ adaptive tabulation (ISAT) [3]. These two measures reduce the computational cost—compared to the direct use of the detailed mechanism—by at least a factor of 1000, making feasible, in days of computer time, calculations which otherwise would have taken years. (In addition to ISAT, other recent storage-retrieval

\* Corresponding author. Fax: +1 607 255 1222.  
E-mail address: [zr26@cornell.edu](mailto:zr26@cornell.edu) (Z. Ren).

algorithms include the repro-modelling [4], piecewise implementation of solution mapping (PRISM) [5], and artificial neural networks (ANN) [6].)

Several different dimension-reduction approaches have been developed for combustion chemistry, among them: the quasi-steady-state approximation (QSSA) [7,8]; rate-controlled constrained equilibrium (RCCE) [9,10]; intrinsic low-dimensional manifolds (ILDM) [11]; trajectory-generated low-dimensional manifolds (TGLDM) [12]; flamelet generated manifolds (FGM) [13]; and the Roussel and Fraser algorithm (RF) [14]. While each approach can claim some success, and several have been extensively applied, all fall short of the ideal, which is as follows. Given a detailed mechanism, a range of conditions, and a specified error tolerance, then, with a minimum of human input, the ideal method achieves the maximum possible dimension reduction while maintaining the specified level of accuracy.

Dimension reduction can be approached from three different but related perspectives. First, one can seek *physical* or *chemical approximations*. For example, in QSSA the approximation is that specified “minor” species are in quasi-steady state. All methods imply that the compositions in the reduced description lie on a low-dimensional manifold in the full composition space. The second perspective, exemplified by ILDM, is to explicitly identify a *low-dimensional manifold*. In most methods, the reduced description is in terms of specified “major” species, and then there is a procedure by which the remaining “minor species” are determined. This provides the third perspective of *species reconstruction*: given the reduced description, how can the full composition (in terms of all species) be determined?

In this paper, we focus on the problem of “species reconstruction,” while making full use of the “low-dimension manifold” perspective. In the next section, we examine the connection between species reconstruction and manifolds; and it is shown that (in conjunction with ISAT) a good species reconstruction procedure is crucial to produce an efficient method for implementing combustion chemistry in various computational fluid dynamics (CFD) applications. Then the method of species reconstruction using pre-image curves is introduced, and its performance is demonstrated for the case of the autoignition of methane.

## 2. Species reconstruction

Every species reconstruction technique corresponds to a procedure for identifying a low-dimension manifold. Among the desirable properties of such manifolds are: existence and uniqueness (for every valid reduced composition); continuity and smoothness; local determination;

and being inertial. Approaches such as QSSA, RCCE, and ILDM are “local” in the sense that, given a particular reduced composition, the corresponding point on the manifold can be determined without constructing the whole or a portion of the manifold. In contrast, TGLM, FGM, and RF require the generation of the entire manifold. Local methods do not require the representation of the manifold and hence are more easily applied in higher dimensions and are more naturally combined with in situ adaptive tabulation.

By definition, a manifold is inertial if the reaction trajectory from any point in the manifold remains in the manifold. For inertial manifolds, the rate of change of the reduced variables is determined by the full chemical kinetics without approximation; whereas, for non-inertial manifolds, the rate of change of the reduced variables depends strongly on the choice of the projection used to project the full rate-of-change vector onto the manifold (see, e.g., [11,15]). Thus, being inertial is a highly desirable property. Of the methods mentioned above, only TGLM and RF yield inertial manifolds. The method presented here is the first which is both local and that yields manifolds which are inertial (to an excellent approximation).

It is important to appreciate the crucial role played by species reconstruction in the implementation of dimension reduction in combination with ISAT in simulations of turbulent combustion. As depicted in Fig. 1, the CFD code—be it direct numerical simulation (DNS), large-eddy simulation (LES) or a probability density function (PDF) method—employs a reduced representation

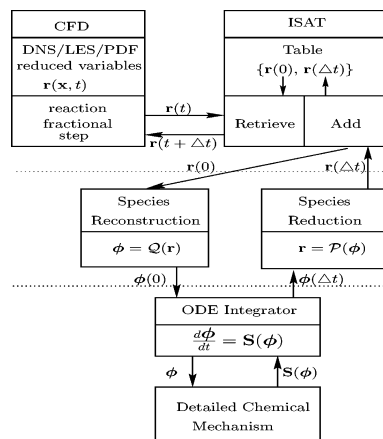


Fig. 1. Schematic of in situ adaptive tabulation in combination with dimension reduction (via species reduction and reconstruction) used in the reaction fractional step of a CFD computation. Above the upper dashed line, all compositions have the reduced representation  $\mathbf{r}$ ; whereas below the lower dashed line all compositions have the full representation  $\phi$ . The operations of species reduction  $\mathcal{P}$  and reconstruction  $\mathcal{Q}$  transform these representations.

of the composition, denoted by  $\mathbf{r}$ , which in the simplest case is the mass fractions of the “major” species. By using a fractional step method (or operator splitting method), we can separate the combustion chemistry from other processes into a reaction fractional step. Given the reduced composition  $\mathbf{r}(t)$  at time  $t$ , the task in this fractional step is to determine the reduced composition  $\mathbf{r}(t + \Delta t)$  after (adiabatic, isobaric) reaction has occurred for the time-step interval  $\Delta t$ . (Since the governing ordinary differential equations (ODEs) are autonomous, the value of  $t$  is immaterial, and without loss of generality we can set  $t = 0$ .) An ISAT table stores pairs of values of  $\mathbf{r}$  before and after reaction  $\{\mathbf{r}(0), \mathbf{r}(\Delta t)\}$ , so that given  $\mathbf{r}(t)$  the corresponding value  $\mathbf{r}(t + \Delta t)$  can be retrieved from the table. As needed, pairs of values  $\{\mathbf{r}(0), \mathbf{r}(\Delta t)\}$  are added to the table by the three-step process shown in Fig. 1. Given the initial reduced composition  $\mathbf{r}(0)$ , species reconstruction is used to obtain the initial full composition, denoted by  $\phi(0)$ . The ODEs governing adiabatic, isobaric reaction (according to the given detailed kinetic mechanism) are integrated for a time  $\Delta t$  to obtain the final full composition  $\phi(\Delta t)$ . Then the final reduced composition  $\mathbf{r}(\Delta t)$  is extracted from  $\phi(\Delta t)$ .

Numerical errors arise in several places in Fig. 1; for example, splitting errors in operator splitting, interpolation errors in ISAT, and numerical integration errors in the ODE solver. But these errors can be reduced at will by reducing the appropriate error tolerances or parameters. For example, the splitting errors can be decreased by decreasing the time step  $\Delta t$  [16]. The only place in this procedure where a non-reducible approximation is made is in the species reconstruction. In other words, apart from controllable numerical errors, the procedure of obtaining  $\mathbf{r}(t + \Delta t)$  from  $\mathbf{r}(t)$  depicted in Fig. 1 would be exact if the species reconstruction were exact. Hence, the crucial importance of species reconstruction.

### 3. Pre-image curves

Corresponding to the conditions of a reaction fractional step, we consider a homogeneous, adiabatic, isobaric system consisting of  $n_s$  chemical species. At time  $t$ , the full composition is represented by the  $n_\phi \equiv n_s + 1$  variables  $\phi(t) \equiv \{\phi_1, \phi_2, \dots, \phi_{n_\phi}\}$ , which are taken to be the species specific moles and enthalpy. Due to chemical reactions, the composition evolves by the autonomous ODE

$$\frac{d\phi(t)}{dt} = \mathbf{S}(\phi(t)), \quad (1)$$

where  $\mathbf{S}$  is the rate of change of composition given by the detailed chemical kinetic mechanism. Except at chemical equilibrium,  $|\mathbf{S}|$  is strictly positive. Moreover, all compositions that occur in the

system satisfy realizability, i.e., they are in the realizable region, which is defined as the  $n_\phi$ -dimensional region of the composition space corresponding to non-negative species specific moles and with the enthalpy corresponding to positive absolute temperatures.

The *reaction mapping*  $\mathbf{R}(\phi, t)$  is defined to be the solution to Eq. (1) after time  $t$ , starting from the initial condition  $\phi$ . From this definition, we have  $\mathbf{R}(\phi, 0) = \phi$ . For  $t$  increasing from zero, in the  $n_\phi$ -dimensional composition space,  $\mathbf{R}(\phi, t)$  represents the reaction trajectory from  $\phi$ , which approaches the chemical equilibrium composition as  $t$  tends to infinity. For  $t$  decreasing from zero,  $\mathbf{R}(\phi, t)$  represents the reaction trajectory from  $\phi$ , going backwards in time; and at some finite (but possibly very large) time  $\tau_b(\phi)$ , this trajectory reaches the boundary of the realizable region on which one or more species vanishes.

Given the full composition  $\phi$ , we consider a reduced composition  $\mathbf{r} = \{r_1, r_2, \dots, r_{n_r}\}$ , where the dimensionality of  $\mathbf{r}$  is less than that of  $\phi$  (i.e.,  $n_r < n_\phi$ ). It is sufficiently general to take the reduction process to be a linear operation. Thus, we consider a specified  $n_\phi \times n_r$  matrix  $\mathbf{B}$  and define the reduction process by

$$\mathbf{r} \equiv \mathbf{B}^T \phi. \quad (2)$$

For example, if  $\mathbf{r}$  consists of specified “major” species, then each column of  $\mathbf{B}$  is a unit vector consisting of a single entry (unity) in the row corresponding to a major species. But more generally, Eq. (2) allows for linear combinations of species (and enthalpy).

The  $n_r$ -dimensional *represented subspace*  $\mathcal{B}$  is defined to be the subspace spanned by the columns of  $\mathbf{B}$ , and its orthogonal complement  $\mathcal{U} = \mathcal{B}^\perp$  is the  $(n_\phi - n_r)$ -dimensional *unrepresented subspace*. Thus, the composition  $\phi$  can be decomposed as  $\phi = \phi^r + \phi^u$ , where  $\phi^r$  and  $\phi^u$  are in  $\mathcal{B}$  and  $\mathcal{U}$ , respectively. It is, in fact, the subspace  $\mathcal{B}$  that is significant, not the particular form of  $\mathbf{B}$ . Hence, without loss of generality, and for simplicity of the following exposition, we take  $\mathbf{B}$  to be orthonormal. Thus,  $\phi^r$  can be written explicitly as  $\phi^r = \mathbf{B}\mathbf{B}^T \phi = \mathbf{B}\mathbf{r}$ .

Given a reduced composition  $\mathbf{r}$ , the full composition  $\phi$  is of course not uniquely determined. We define a composition  $\phi$  to be *feasible* (for given  $\mathbf{r}$ ) if it satisfies both realizability and  $\mathbf{B}^T \phi = \mathbf{r}$ , and the union of all feasible compositions is called the *feasible region*, denoted by  $\mathcal{F}(\mathbf{r})$ . For given  $\mathbf{r}$ , every feasible composition can be written as  $\phi = \mathbf{B}\mathbf{r} + \phi^u$ , where  $\phi^u$  is in  $\mathcal{U}$ , showing that  $\mathcal{F}(\mathbf{r})$  lies in an  $(n_\phi - n_r)$ -dimensional affine space (i.e., the subspace  $\mathcal{U}$  shifted from the origin by the vector  $\mathbf{B}\mathbf{r}$ ). The problem of species reconstruction is to select from the feasible region the particular composition which is deemed to be most likely to occur in a reactive flow.

The method of species reconstruction introduced in this work is based on pre-image curves. To develop the concepts involved, we first define pre-image points and the pre-image manifold.

Given a reduced composition  $\mathbf{r}$ , a pre-image point of  $\mathbf{r}$  is a composition  $\phi$ , which satisfies both realizability and the condition  $\mathbf{B}^T \mathbf{R}(\phi, t) = \mathbf{r}$  for some positive  $t$ . For positive  $t$ ,  $\mathbf{R}(\phi, t)$  is the reaction trajectory (forward in time) from the initial point  $\phi$ ; and  $\mathbf{B}^T \mathbf{R}(\phi, t)$  is the projection of this trajectory onto the reduced subspace. Thus, by definition,  $\phi$  is a pre-image point of  $\mathbf{r}$  if the projection of the trajectory from  $\phi$  onto the reduced subspace passes through  $\mathbf{r}$  at some positive time  $t$ .

The pre-image manifold of  $\mathbf{r}$ , denoted by  $\mathcal{M}_P(\mathbf{r})$ , is defined as the union of all pre-image points of  $\mathbf{r}$ . In principle, this manifold can be generated by following trajectories backwards from feasible compositions. Thus, we have  $\mathcal{M}_P(\mathbf{r}) = \{\phi : \phi = \mathbf{R}(\phi^f, -t), \phi^f \in \mathcal{F}(\mathbf{r}), 0 \leq t \leq \tau_b(\phi^f)\}$ . It follows from the well-known properties of ODEs that  $\mathcal{M}_P(\mathbf{r})$  is an  $(n_\phi - n_r + 1)$ -dimensional inertial manifold.

Figure 2 is a sketch of reaction trajectories in the pre-image manifold. The represented subspace  $\mathcal{B}$  and the unrepresented subspace  $\mathcal{U}$  are each represented by a single axis. For the situation depicted, there is a strongly attracting manifold (bold line), which is a well-established characteristic of combustion systems. We argue that, ideally, the species reconstruction method should identify the composition denoted “ $A$ ,” which is the intersection of the attracting manifold and the feasible region. As may be observed, because of the attrac-

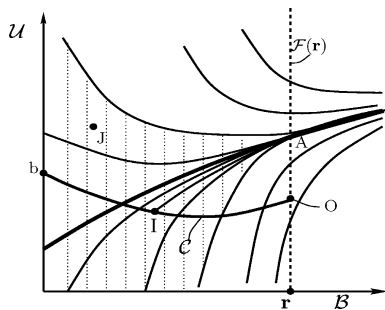


Fig. 2. Sketch of the composition space indicated by the represented subspace  $\mathcal{B}$  and the unrepresented subspace  $\mathcal{U}$ . The dashed line is the feasible region  $\mathcal{F}(\mathbf{r})$  corresponding to the reduced composition  $\mathbf{r}$ ;  $\mathcal{C}$  is the pre-image curve starting at  $O$  and ending at  $b$ , on the boundary of the realizable region. The other curves are reaction trajectories, which intersect  $\mathcal{F}(\mathbf{r})$ . There is a strongly attracting manifold (bold line) so that all trajectories originating in the shaded region intersect  $\mathcal{F}(\mathbf{r})$  close to the point  $A$ . (Note that, although they are depicted as lines,  $\mathcal{B}$ ,  $\mathcal{U}$ , and  $\mathcal{F}(\mathbf{r})$  are of dimensions  $n_r$ ,  $n_\phi - n_r$ , and  $n_\phi - n_r + 1$ , respectively.)

tion of the manifold, trajectories from a sizeable region of the pre-image manifold (the shaded area in Fig. 2) intersect the feasible region quite close to  $A$ . A good approximation to the point  $A$  can therefore be obtained by following the reaction trajectory from a point such as  $I$  in Fig. 2 until it intersects the feasible region. Furthermore, again as a property of strongly attracting manifolds, the approximation thus obtained is insensitive to the precise location of the initial point. For example, the approximation obtained by using  $J$  instead of  $I$  as the initial point is little different.

The next step is to determine a suitable initial point  $I$ . This is achieved by generating a curve  $\mathcal{C}$  in the pre-image manifold from a starting feasible point, denoted by  $O$  in Fig. 2. This pre-image curve  $\mathcal{C}$  is parameterized by the arclength  $s$  measured from  $O$ , and the composition on the curve is denoted by  $\hat{\phi}(\mathbf{r}, s)$ , or simply  $\hat{\phi}(s)$ . Thus, the starting point  $O$  of the curve is  $\hat{\phi}^0 = \hat{\phi}(0)$ , and the initial point  $I$  of the reaction trajectory is  $\hat{\phi}^I = \hat{\phi}(s^*)$ , for specified  $s^*$ .

#### 4. Construction of the minimum curvature pre-image curve

There are several ways to generate pre-image curves. In this section, we describe the construction of *minimum-curvature pre-image curve*, which has been implemented and tested, as reported below. In this method, for given  $\mathbf{r}$ , the pre-image curve is started from the corresponding point on the constrained equilibrium manifold (CEM)  $\mathcal{M}_{CE}$ , denoted by  $\phi^{CE}(\mathbf{r})$ , which is the feasible composition of maximum entropy. This manifold has impeccable mathematical properties, and efficient methods for its computation are well-established [17]. With the initial tangent vector  $\hat{\phi}'(0) \equiv [d\hat{\phi}(s)/ds]_{s=0}$  being in the tangent space of the CEM and in a direction opposing reaction (i.e.,  $\hat{\phi}'(0)^T \mathbf{S}(\hat{\phi}(0)) < 0$ ), the curve is continued with minimum possible curvature. Hence, we refer to the result as the *minimum-curvature pre-image curve*.

Given the minimum-curvature pre-image curve  $\hat{\phi}(s)$  for some given  $s$ , we describe here the determination of  $\hat{\phi}(s + ds)$ , for positive, infinitesimal  $ds$ . Thus, starting from the initial conditions,  $\hat{\phi}(0)$  and  $\hat{\phi}'(0)$ , the whole curve  $\mathcal{C}$  can be generated, up to the boundary of the realizable region.

Some preliminary results are shown without derivation here. First, the sensitivity (to initial condition) matrix  $\mathbf{A}(\phi, t)$  is defined by

$$A_{ij}(\phi, t) \equiv \frac{\partial R_i(\phi, t)}{\partial \phi_j}. \quad (3)$$

In practice, the reaction mapping  $\mathbf{R}(\phi, t)$  and sensitivity matrix  $\mathbf{A}(\phi, t)$  are obtained together by

solving Eq. (1) using the DDASAC code (Caracotsios and Stewart, 1995). Second, the derivative of the reaction mapping  $\mathbf{R}(\phi, t)$  is

$$\frac{\partial \mathbf{R}(\phi, t)}{\partial t} = \mathbf{S}(\mathbf{R}[\phi, t]) = \mathbf{A}\mathbf{S}(\phi). \quad (4)$$

Every point in  $\mathcal{C}$  is a pre-image point, and hence, satisfies the relation

$$\mathbf{B}^T \mathbf{R}(\hat{\phi}(s), \tau(s)) = \mathbf{B}^T \hat{\phi}(0) = \mathbf{r}, \quad (5)$$

where  $\tau(s)$  is the time along the reaction trajectory at which it intersects the feasible region. Differentiating this relation with respect to  $s$ , we obtain the result used below

$$\mathbf{B}^T \mathbf{A}[\hat{\phi}'(s) + \mathbf{S}(\hat{\phi}(s))\tau'(s)] = 0, \quad (6)$$

where use has been made of Eqs. (3) and (4), and  $\tau'(s)$  is defined as  $\tau'(s) = d\tau(s)/ds$ .

To generate the infinitesimal extension of the minimum-curvature pre-image curve, we write the composition at arclength  $s + ds$  as

$$\hat{\phi}(s + ds) = \hat{\phi}(s) + \hat{\phi}'(s)ds + \delta\phi, \quad (7)$$

which implicitly defines  $\delta\phi$ . The first two terms on the right-hand side represent the straight-line extension of the curve; and, providing that the curve is regular at  $s$ , comparison with the Taylor series about  $s$  reveals that  $\delta\phi$  is of order  $ds^2$ , and its magnitude is proportional to the curvature,  $|\hat{\phi}''(s)|/|\hat{\phi}'(s)|$ . This small departure  $\delta\phi$  from straight-line behavior is uniquely determined by the requirements that  $\hat{\phi}(s + ds)$  is, indeed, a pre-image point, and that  $|\delta\phi|$  is as small as possible. The first requirement is enforced by applying Eq. (5) at  $s + ds$ . Thus, we substitute Eq. (7) into Eq. (5) and perform a Taylor series expansion about  $\hat{\phi}(s) + \hat{\phi}'(s)ds$ ,  $\tau(s) + \tau'(s)ds$  to obtain

$$\begin{aligned} 0 &= \mathbf{B}^T \mathbf{R}(\hat{\phi}(s + ds), \tau(s + ds)) - \mathbf{B}^T \mathbf{R}(\hat{\phi}(s), \tau(s)) \\ &= \mathbf{B}^T \mathbf{R}(\hat{\phi} + \hat{\phi}' ds + \delta\phi, \tau + \tau' ds + \delta\tau) - \mathbf{B}^T \mathbf{R}(\hat{\phi}, \tau) \\ &= \mathbf{B}^T \{ \mathbf{R}(\hat{\phi} + \hat{\phi}' ds, \tau + \tau' ds) - \mathbf{R}(\hat{\phi}, \tau) \} \\ &\quad + \mathbf{B}^T \mathbf{A}[\delta\phi + \mathbf{S}\delta\tau] \\ &= \mathbf{B}^T \mathbf{A}[\delta\phi + \mathbf{S}\delta\tau + \mathbf{A}^{-1}\delta\mathbf{R}]. \end{aligned} \quad (8)$$

Here,  $\delta\mathbf{R}$  is defined by the quantity in braces in the penultimate line, and  $\delta\tau$  is defined as  $\delta\tau = \tau(s + ds) - [\tau(s) + \tau'(s)ds]$ . It is readily shown that  $\delta\phi$ ,  $\delta\mathbf{R}$ , and  $\delta\tau$  are each of order  $ds^2$  (provided that the curve is regular at  $s$ ).

In the last line of Eq. (8), given  $\hat{\phi}(s)$ ,  $\hat{\phi}'(s)$ , and  $ds$ , all quantities are determined except for  $\delta\phi$  and  $\delta\tau$ . Thus, Eq. (8) represents an underdetermined set of  $n_r$  equations in  $n_\phi + 1$  unknowns. We take the solution (for  $\delta\phi$  and  $\delta\tau$ ) which minimizes  $|\delta\phi|$  and thereby minimizes the local curvature.

With  $\delta\phi$  having thus been determined, the curve is extended to  $\hat{\phi}(s + ds)$  by Eq. (7). It is expected and found that the curve is regular, but

even if this were not the case, a unique minimum norm solution for  $\delta\phi$  is guaranteed to exist. Hence, it is guaranteed that there is a unique minimum-curvature pre-image curve extending from the starting point  $\hat{\phi}(0)$  to a point on the boundary of the realizable region, denoted by “ $b$ ” in Fig. 2.

This differential construction of the minimum-curvature pre-image curve forms the basis for a convergent numerical algorithm. Using a finite arclength increment  $\Delta s$ , the analog of Eq. (8) is used to obtain an initial estimate for  $\hat{\phi}(s + \Delta s)$ . Newton’s method is then used to refine this solution, to ensure that it is a pre-image point.

Given  $\mathbf{r}$  and the pre-image curve  $\hat{\phi}(s)$ , we define  $\phi^M(s) \equiv \mathbf{R}(\hat{\phi}(s), \tau(s))$  to be the feasible composition, which is mapped from the pre-image curve (as a function of arclength  $s$ ). For  $s = 0$ , we have  $\phi^M(0) = \hat{\phi}(0) = \phi^{CE}(\mathbf{r})$ . As the results below confirm, as  $s$  increases,  $\phi^M(s)$  tends to an asymptote, which is maintained to the end of the curve ( $s = s_b$ ). Once the asymptote is reached,  $\phi^M(s)$  is insensitive to perturbations (within the pre-image manifold) of the pre-image point.

We denote by  $s^*$  a specified point on the pre-image curve in the asymptotic region, and define the *reconstructed composition* by  $\phi^R(\mathbf{r}) \equiv \mathbf{R}(\hat{\phi}(\mathbf{r}, s^*), \tau(\mathbf{r}, s^*))$ . In this work, for simplicity, we take  $s^* = s_b$  (i.e., the end of the pre-image curve), but it would be computationally more efficient to take a smaller value. The union (for all  $\mathbf{r}$ ) of the reconstructed composition  $\phi^R(\mathbf{r})$ , denoted by  $\mathcal{M}_R$ , is the *reconstructed manifold* from the minimum-curvature pre-image curve. It should be noted that the reconstructed manifold  $\mathcal{M}_R$  (like  $\mathcal{M}_{CE}$ ) depends solely on the specified represented subspace  $\mathcal{B}$ .

## 5. Results

To demonstrate the performance of the species reconstruction method, and to quantify its accuracy, we take as a test case the autoignition of methane.

The detailed methane mechanism employed is GRI 1.2<sup>1</sup> [18], which involves 4 elements, 31 species, and 175 reactions. Nitrogen chemistry is not included so that  $\text{N}_2$  is considered to be inert. The initial composition (approximating stoichiometric methane–air) is taken to be (in relative volume units)  $\text{N}_2$  (71.5),  $\text{O}_2$  (19),  $\text{CH}_4$  (9.5),  $\text{CO}_2$  (3), and  $\text{H}_2\text{O}$  (2); the initial temperature is 1500 K; and the pressure is atmospheric throughout. From this initial condition, Eq. (1) is directly integrated to yield the composition as a function

<sup>1</sup> This older mechanism is used to facilitate comparison with previous work using different reduction techniques, e.g., [10].

of time, which is denoted by  $\phi^{\text{DI}}(t)$ . During this autoignition process, pressure, enthalpy, and the mass fractions of the four elements remain fixed, and hence, the composition has  $(31 - 4) = 27$  degrees of freedom.

At different times  $t$  during the autoignition, the species reconstruction methodology is applied (based on the reduced composition  $\mathbf{B}^T \phi^{\text{DI}}$ ), and the reconstructed composition  $\phi^{\text{R}}$  is compared to  $\phi^{\text{DI}}$ .

The reconstructed composition depends on the represented subspace  $\mathcal{B}$  spanned by the columns of the matrix  $\mathbf{B}$ . We consider two cases, denoted by  $\mathbf{B}_4$  and  $\mathbf{B}_6$ , which involve four and six reduced variables (in addition to the fixed enthalpy and the fixed mass fractions of the four elements). In  $\mathbf{B}_4$ , the reduced variables are the “major” species  $\text{CH}_4$ ,  $\text{O}_2$ ,  $\text{CO}_2$ , and  $\text{H}_2\text{O}$ ; and in  $\mathbf{B}_6$  two more species are added, namely  $\text{CO}$  and  $\text{H}_2$ . Thus, in terms of the number of degrees of freedom, the dimension reduction achieved by these two cases is from 27 to 4 and 6 degrees of freedom, respectively.

In Fig. 3, we examine various properties of the pre-image curve  $\phi(s)$  and of the corresponding mapped composition  $\phi^{\text{M}}(s)$ , at a particular time, namely when the temperature is  $T^{\text{DI}} = 1852.6$  K. Given the full composition  $\phi^{\text{DI}}$ , for each of the cases  $\mathbf{B}_4$  and  $\mathbf{B}_6$ , the reduced composition  $\mathbf{r}$  is obtained (as  $\mathbf{r} = \mathbf{B}^T \phi^{\text{DI}}$ ), and then the pre-image curves are generated. As a function of arclength  $s$ , the top row of plots in Fig. 3 shows the time  $\tau(s)$ , and the specific moles of  $\text{H}_2\text{O}$  and  $\text{H}$  on the pre-image curve. It is interesting to observe the differences between  $\mathbf{B}_4$  and  $\mathbf{B}_6$ , especially for  $\text{H}$ , and that (inevitably) the composition changes significantly along the curves. In the second row

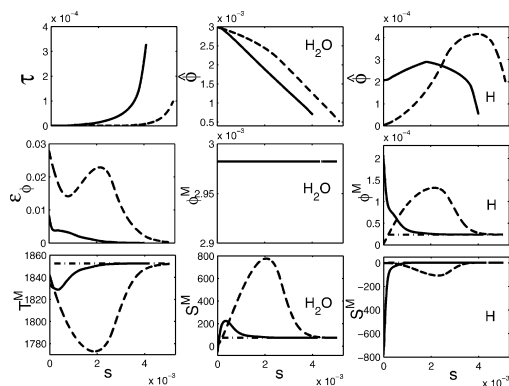


Fig. 3. Properties,  $\tau(s)$  and  $\hat{\phi}(s)$ , of the pre-image curve (top row); the reconstruction error  $\varepsilon_\phi(s)$  and the mapped composition  $\phi^{\text{M}}(s)$  (middle row); the mapped temperature  $T^{\text{M}}(s)$  and rate of change  $S^{\text{M}}(s)$  (bottom row). Solid line,  $\mathbf{B}_6$ ; dashed line,  $\mathbf{B}_4$ ; dot-dashed line, direct integration (DI). For the case  $T^{\text{DI}} = 1852.6$  K. Units:  $\tau$  (s),  $T$  (K),  $\phi$  and  $s$  (k mol/kg), and  $S$  (k mol/kg/s).

of plots, the corresponding mapped compositions are shown for  $\text{H}_2\text{O}$  and  $\text{H}$ . Since  $\text{H}_2\text{O}$  is a reduced variable (in both  $\mathbf{B}_4$  and  $\mathbf{B}_6$ ), inevitably we have  $\phi_{\text{H}_2\text{O}}^{\text{M}}(s) = \phi_{\text{H}_2\text{O}}^{\text{DI}}$  for all  $s$  (even though  $\hat{\phi}_{\text{H}_2\text{O}}(s)$  varies appreciably).

In confirmation of the ideas behind the pre-image curve approach, it may be seen that  $\phi_{\text{H}}^{\text{M}}(s)$  approaches an asymptote—sooner for  $\mathbf{B}_6$  than for  $\mathbf{B}_4$ —and that the asymptotic value is very close to  $\phi_{\text{H}}^{\text{DI}}$ . The approach of  $\phi^{\text{M}}(s)$  to  $\phi^{\text{DI}}$  is confirmed in the left-hand center plot, which shows the normalized species reconstruction error

$$\varepsilon_\phi(s) \equiv |\phi^{\text{M}}(s) - \phi^{\text{DI}}|/|\phi^{\text{DI}}|. \tag{9}$$

Note that  $\varepsilon_\phi(0)$  represents the error in species reconstruction using RCCE. As may be seen, as  $s$  increases  $\varepsilon_\phi(s)$  becomes very small (as further quantified below); and, as expected, the error is substantially less for  $\mathbf{B}_6$  than it is for  $\mathbf{B}_4$ . The final row of plots in Fig. 3 shows the mapped temperature  $T^{\text{M}}(s)$  and rates of change  $S^{\text{M}} = S(\phi^{\text{M}})$ , for  $\text{H}_2\text{O}$  and  $\text{H}$ , which also converge to the direct-integration values.

Figure 4 provides further quantification of the reconstruction errors, over a range of temperatures during autoignition. This includes the case  $T^{\text{DI}} = 1502.35$  K, in the early stages of autoignition, which is challenging to species reconstruction.

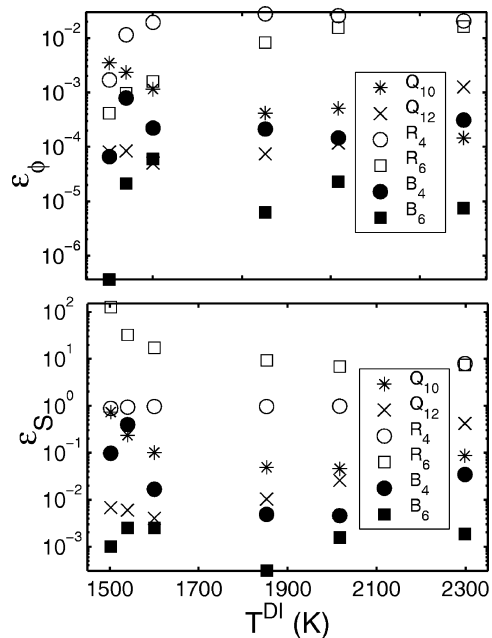


Fig. 4. Normalized error in reconstructed species ( $\varepsilon_\phi(s^*)$ , Eq. (9), upper plot) and in reconstructed rate of change ( $\varepsilon_S$ , Eq. (10), lower plot) at different temperatures  $T^{\text{DI}}$  during autoignition. QSSA,  $Q_{10}$ ,  $Q_{12}$ ; RCCE,  $R_4$ ,  $R_6$ ; and pre-image curve  $\mathbf{B}_4$ ,  $\mathbf{B}_6$ .

tion methodologies. As may be seen from the upper plot in Fig. 4, for  $B_4$  and  $B_6$ , the reconstruction error  $\varepsilon_\phi$  (with  $s = s^* = s_b$ ) is everywhere less than  $10^{-3}$  and  $10^{-4}$ , respectively. The error in the reconstructed rate of change

$$\varepsilon_S \equiv |\mathbf{S}(\phi^M(s^*)) - \mathbf{S}(\phi^{DI})|/|\mathbf{S}(\phi^{DI})| \quad (10)$$

(shown in the lower plot) is somewhat larger, but is nevertheless less than  $\frac{10\%}{2}$  for  $B_6$ .

For comparison, Fig. 4 also shows the reconstruction errors incurred by RCCE (using the same reduced variables and denoted by  $R_4$  and  $R_6$ ) and by two QSSA methods denoted by  $Q_{10}$  and  $Q_{12}$ . The first one,  $Q_{10}$ , corresponds to the reduced mechanism of [19], which has 14 major (i.e., non-steady-state) species; and the second,  $Q_{12}$ , corresponds to ARMI [2], which has 16 major species. Given that there are 4 elements, these reduced descriptions have 10 and 12 degrees of freedom, respectively. Given the major species from  $\phi^{DI}$ , the minor species are reconstructed from the quasi-steady-state approximation. As may be seen from Fig. 4, the pre-image curve method yields errors  $\varepsilon_\phi$  typically 2 orders of magnitude smaller than RCCE, and errors  $\varepsilon_S$  typically 3 (or more) orders of magnitude smaller. With just 6 degrees of freedom,  $B_6$  produces smaller reconstruction errors than  $Q_{10}$  and  $Q_{12}$ , which have 10 and 12 degrees of freedom.

An important property of the reconstructed manifold  $\mathcal{M}_R$  is that it is inertial—to an excellent approximation. To substantiate this claim, we report the angle between the reaction rate  $\mathbf{S}(\phi^R)$  and the tangent space of the manifold  $\mathcal{M}_R$ . (This angle is obtained numerically (for small  $\delta t$ ) as the angle between the vectors  $\delta\mathbf{R} \equiv [\mathbf{R}(\phi^R, \delta t) - \phi^R]$  and  $[\phi^R(\mathbf{r} + \delta\mathbf{r}) - \phi^R(\mathbf{r})]$ , for  $\delta\mathbf{r} \equiv \mathbf{B}^T \delta\mathbf{R}$ .) For  $B_4$ , at the two lower temperatures ( $T^{DI} < 1650$  K) the angle  $\theta$  is less than  $3^\circ$ ; whereas at the other 4 temperatures investigated  $\theta$  is less than  $1^\circ$ .

## 6. Conclusions

The computational cost of using detailed chemical kinetics can be reduced by many orders of magnitude through the combined approaches of dimension reduction and storage-retrieval. From one of several useful perspectives, the key to dimension reduction is “species reconstruction”. And the accuracy of the combined dimension-reduction/storage-retrieval approach is fundamentally determined by the accuracy of the species reconstruction.

The species reconstruction method presented here is based on the minimum-curvature pre-image curve  $\mathcal{C}$ . With the starting point  $\hat{\phi}(0)$  and the initial direction  $\hat{\phi}'(0)$  being specified in the constrained equilibrium manifold  $\mathcal{M}_{CE}$ , the curve is continued, with minimal curvature, subject to the requirement

that each point on the curve is a pre-image point, until the boundary of the realizable region is reached. The method is demonstrated and tested for the autoignition of methane using a detailed mechanism with 31 species, 4 elements, and therefore 27 degrees of freedom. Two reduced representations are used, denoted by  $B_4$  and  $B_6$ , which have 4 and 6 degrees of freedom, respectively. It is shown that the composition  $\phi^M(s)$  mapped from the pre-image curve converges to an asymptote as  $s$  increases, which closely corresponds to the full composition  $\phi^{DI}$  obtained from the detailed chemistry calculation. The normalized errors incurred in the reconstruction of the composition, and of its rate of change are very small—e.g.,  $10^{-4}$  and  $5 \times 10^{-3}$ , respectively, for  $B_6$ . These errors are two orders of magnitude less than those incurred in RCCE (with the same degrees of freedom), and are less than those incurred by QSSA with 10 and 12 degrees of freedom.

The union of reconstructed compositions (for all reduced compositions) is the reconstructed manifold  $\mathcal{M}_R$ ; and it is shown that this manifold is inertial (to an excellent approximation). This pre-image curve species reconstruction method is, therefore, the first approach, which locally determines points on a low-dimensional inertial manifold.

The reconstructed manifold depends on: the reduced representation (which is specified by the  $n_\phi \times n_r$  matrix  $\mathbf{B}$ ); the method of generating the pre-image curve; and the specific point  $s^*$  used to obtain the reconstructed composition (i.e.,  $\phi^R \equiv \phi^M(s^*)$ ). In future work, we will investigate different ways of generating pre-image curves, and automatic ways to determine optimal choices of  $\mathbf{B}$  and  $s^*$ . In addition, more comprehensive testing will be performed, with a variety of mechanisms, and for a variety of combustion problems, including laminar flames. Finally, a computationally efficient implementation of the method will be combined with ISAT for application to the simulation and modelling of turbulent combustion.

## Acknowledgment

This work is supported by Department of Energy, Grant No. DE-FG02-90ER14128.

## References

- [1] Q. Tang, J. Xu, S.B. Pope, *Proc. Combust. Inst.* 28 (2000) 133–139.
- [2] C.J. Sung, C.K. Law, J.-Y. Chen, *Proc. Combust. Inst.* 27 (1998) 295–304.
- [3] S.B. Pope, *Combust. Theory Modelling* 1 (1997) 41–63.
- [4] T. Turányi, *Proc. Combust. Inst.* 25 (1994) 949–955.

- [5] J.B. Bell, N.J. Brown, M.S. Day, M. Frenklach, J.F. Grcar, R.M. Propp, S.R. Tonse, *Proc. Combust. Inst.* 28 (2000) 107–113.
- [6] F.C. Christo, A.R. Masri, E.M. Nebot, *Combust. Flame* 106 (1996) 406–427.
- [7] M. Bodenstein, S.C. Lind, *Z. Phys. Chem.* 57 (1906) 168.
- [8] M.D. Smooke (Ed.), *Reduced Kinetic Mechanisms and Asymptotic Approximations for Methane–Air Flames, Lecture Notes in Physics*, vol. 384. Springer, Berlin, 1991.
- [9] J.C. Keck, *Prog. Energy Combust. Sci.* 16 (1990) 125–154.
- [10] Q. Tang, S.B. Pope, *Proc. Combust. Inst.* 29 (2002) 1411–1417.
- [11] U. Maas, S.B. Pope, *Combust. Flame* 88 (1992) 239–264.
- [12] S.B. Pope, U. Maas, *Simplifying chemical kinetics: trajectory-generated low-dimensional manifolds*. FDA 93-11, Cornell University, 1993.
- [13] J.A. van Oijen, L.P.H. de Goeij, *Combust. Sci. Technol.* 161 (2000) 113–137.
- [14] M.R. Roussel, S.J. Fraser, *J. Phys. Chem.* 97 (1993) 8316–8327.
- [15] Q. Tang, S.B. Pope, *Combust. Theory Modelling* 8 (2004) 255–279.
- [16] B. Yang, S.B. Pope, *Combust. Flame* 112 (1–2) (1998) 16–32.
- [17] W.C. Reynolds, *The Element Potential Method for Chemical Equilibrium Analysis: Implementation in the Interactive Program STANJAN*, Technical report, Stanford University, 1986.
- [18] M. Frenklach, H. Wang, M. Goldenberg, G.P. Smith, D.M. Golden, C.T. Bowman, R.K. Hanson, W.C. Gardiner, V. Lissianski, *GRI-Mech: An Optimized Detailed Chemical Reaction Mechanism for Methane Combustion*, Gas Research Institute Topical Report, Gas Research Institute, Chicago, 1995.
- [19] T. Lu, Y. Ju, C.K. Law, *Combust. Flame* 126 (1–2) (2001) 1445–1455.

## Comments

*Tianfeng Lu, Princeton University, USA.* The 10-step QSSA based reduced mechanism for CH<sub>4</sub> was developed with PSR for burning cases, and it should not be applied for an ignition study. It would be more convincing if the new method in the present work could be compared with the QSSA reduction within the parameter range for the QSS reduction.

*Reply.* Besides the 10-step QSSA, in this paper, the new method is also compared with the 12-step QSSA (ARMI), which is widely tested including the auto-ignition case.

●

*Weiyong Tang, University of Illinois at Chicago, USA.* You use a feasible trust region. Is it pre-assigned or “automatically” computationally generated?

*Reply.* The feasible region is mathematically well defined in the composition space for a given reduced composition. The definition for the feasible region is given in the paper on page 7, paragraph 3.